Journal of Alloys and Compounds 486 (2009) 29–36

Contents lists available at ScienceDirect

Journal of Alloys and Compounds

journal homepage: www.elsevier.com/locate/jallcom

$LFe_6Sn_4Ge_2$ (L = Dy, Ho, Er) studied by neutron diffraction and Mössbauer spectroscopy

Laura K. Perry[a], D.H. Ryan[a], G. Venturini[b,*], B. Malaman[b]

[a] Centre for the Physics of Materials and Physics Department, McGill University, 3600 University Street, Montréal, Quebec H3A 2T8, Canada
[b] Laboratoire de Chimie du Solide Minéral, Institut Jean Lamour (UMR 7198) Faculté des Sciences et Techniques, B.P. 239, 54506 Vandoeuvre les Nancy Cedexs, France

ARTICLE INFO

Article history:
Received 17 June 2009
Accepted 3 July 2009
Available online 29 July 2009

Keywords:
Lanthanoid alloys and compounds
Transition metal alloys and compounds
Mössbauer spectroscopy
Neutron diffraction

ABSTRACT

The compounds $LFe_6Sn_4Ge_2$ (L = Dy, Ho, Er) have been studied by neutron diffraction and ^{119}Sn Mössbauer spectroscopy. At room temperature the magnetic structure consists of ferromagnetic Fe (0 0 1) planes which are coupled antiferromagnetically along the stacking direction, with the moments aligned along the hexagonal *c* axis. The lanthanoid sublattice orders around T_t = 21 and 11 K for the Dy and Ho compounds respectively. The erbium moment is not ordered at 1.7 K. Below T_t, $LFe_6Sn_4Ge_2$ (L = Dy, Ho) display a helimagnetic structure with propagation vectors of (0, 0, 0.1262) and (0, 0, 0.1559) respectively. Ordering of the Dy and Ho moments causes a small distorsion of the high temperature AF structure of the iron sublattice and the development of a weak helimagnetic component (0.33 and 0.27 μ_B respectively). The orientation of the iron component with respect to the L moments suggests that the main magnetic interaction between the two sublattice takes place between the L plane and the next nearest Fe planes.

1. Introduction

Although the orthorhombic LFe_6X_6 compounds (L = lanthanoid, X = Ge, Sn) display unique behaviour among the intermetallic compounds: the independent ordering of the Fe and lanthanoid sublattices [1–4], a recent study of hexagonal $TbFe_6Sn_4Ge_2$ pseudo-ternary compound has shown that a slight modification of the iron magnetic order occurs at the ordering point of the lanthanoid sublattice [5]. This transition is characterized by a helimagnetic ordering of the terbium moments and the concomitant development of a helimagnetic component on the iron sublattice. In order to better understand this phenomenon, an investigation of the magnetic properties of other Ge-stabilized hexagonal $LFe_6Sn_4Ge_2$ (L = Dy–Er) has been undertaken by neutron diffraction and Mössbauer spectroscopy.

2. Experimental methods

The samples were prepared in an induction furnace starting from stoichiometric amounts of the elements. The resulting ingots were annealed at 1123 K for 1 week, ground compacted again and annealed for one more week. The samples were checked by conventional X-ray powder analysis (Guinier Co Kα). The main systematic impurity lines detected were those of elemental tin, L_2O_3 and hexagonal Fe_3Ge. The erbium compound seemed to contain additional weak amounts of impurities indexed as a Ni_2In-type $Fe_{2-x}Ge$ alloy and a $CeNiSi_2$-type $ErFe_xSn_2$ compound [6].

The neutron diffraction patterns were recorded on the D1B diffractometer at the Institut Laue Langevin (Grenoble) using the wavelength (λ = 2.520 Å). Two long duration patterns were recorded at 300 and 2 K and short duration patterns in the 2–50 K temperature range to check the variation of the Bragg angles and intensity. Refinements were done using the FULLPROF software [7].

^{119}Sn Mössbauer spectra were collected in transmission mode on a constant acceleration spectrometer using a 0.4 GBq ^{119m}Sn CaSnO3 source with the sample in a helium flow cryostat. A 25 μm Pd filter was used to absorb the Sn Kα X-rays also emitted by the source. The spectrometer was calibrated using a ^{57}CoRh source and a α-Fe foil. Typical line widths were 0.85 mm/s full width at half maximum (FWHM), somewhat broader than the 0.6 mm/s obtained using a $CaSnO_3$ standard. Isomer shifts were measured relative to the same $CaSnO_3$ standard. The spectra were fitted using a conventional non-linear least-squares minimisation routine to a sum of Lorentzian line shapes. As the magnetic hyperfine fields (B_{hf}) at the Sn(2d) sites were quite small, and thus comparable to the quadrupole interaction, line positions and intensities were calculated using a full solution to the nuclear Hamiltonian [8]. Each spectrum was fitted with three components: a well-split magnetic sextet ($B_{hf} \approx 20$ T at 5 K), corresponding to tin atoms in the Sn(2e) site, and a quadrupole-split doublet attributed to tin in the Sn(2d) site accounted for over 90% of the observed area, with a singlet associated with a metallic tin impurity completing the fit. The area of this last component was strongly temperature dependent, becoming much larger at low temperatures as expected from the low Debye temperature of metallic tin. The contribution of minority tin in the Sn(2c) sites was not included as these sites are known to be occupied almost entirely by germanium and no additional feature was apparent in the spectra.

3. Results

3.1. Crystal structure

The neutron diffraction patterns of the $LFe_6Sn_4Ge_2$ samples clearly display the typical lines of the $HfFe_6Ge_6$ type structure

* Corresponding author. Tel.: +33 3 83 68 46 73; fax: +33 3 83 68 46 11.
E-mail address: Gerard.Venturini@lcsm.uhp-nancy.fr (G. Venturini).

0925-8388/$ – see front matter © 2009 Elsevier B.V. All rights reserved.
doi:10.1016/j.jallcom.2009.07.022

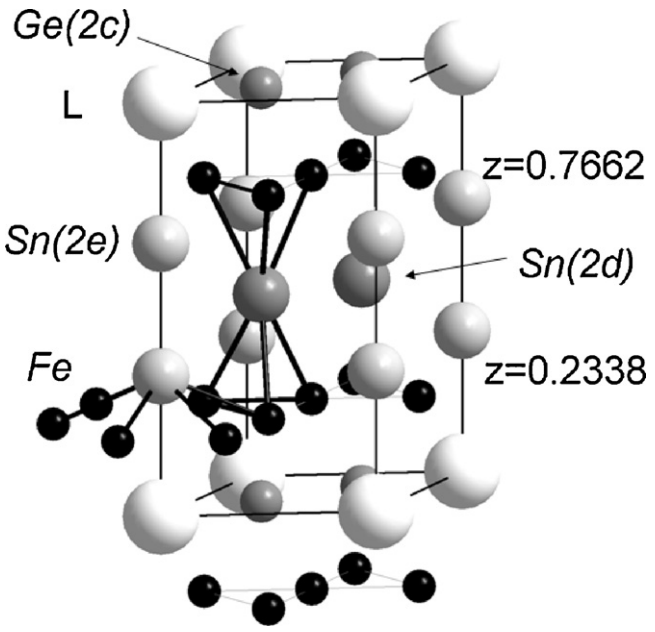

Fig. 1. Crystal structure of the $LFe_6Sn_4Ge_2$ compounds (the iron coordination of the Sn atoms is outlined).

[*P*6/*mmm*; Hf in 1(a) (0, 0, 0); Fe in 6(i) (1/2, 0, *z*); Ge in 2(c) (1/3, 2/3, 0), 2(d) (1/3, 2/3, 1/2) and 2(e) (0, 0, *z*)] (Fig. 1). Previous studies indicated that the Ge atoms were mainly located in the 2(c) site [9]. This distribution was confirmed for the room temperature data. A preliminary refinement was done starting with the Sn atoms in the 2(d) and 2(e) sites and the Ge atoms in the 2(c) site and then refining the occupancy factors. In each case, we found that the occupation of the 2(c) site decreases slightly. According to the relative Fermi lengths of tin (6.225 fm) and germanium (8.185 fm), this means that the 2(c) site is partly occupied by tin atoms. The occupation of the 2(e) site is always close to the ideal value or slightly weaker, indicating that a full occupation of this site by tin could be assumed. This occupation was fixed in the final refinements. In the case of the Dy and Ho compounds, the occupancy factor of Sn in site 2(d) exhibited a weak increase indicating a possible substitution by germanium while it decreases slightly in the Er compound. The final refinements with the relative occupation by tin and germanium atoms are given in Table 1. In all cases, we observed a strong shift of the z_{Fe} coordinate from the idealized 1/4 value. This means that the Fe planes move towards the 2(c) site (1/3, 2/3, 0) occupied by the small Ge atoms yielding Fe–2(c) distances that are much shorter than the Fe–2(d) distances. As a result, the Fe–Fe interplane distances are shorter in the Fe–2(c)–Fe slab than in the Fe–2(d)–Fe slab.

Table 1
Crystallographic and magnetic parameters of $LFe_6Sn_4Ge_2$ refined at 300 K.

L	Dy	Ho	Er
a (Å)	5.2746(6)	5.2797(5)	5.2787(7)
c (Å)	8.635(1)	8.644(1)	8.667(1)
z_{Sn}	0.339(1)	0.337(1)	0.335(1)
z_{Fe}	0.2338(6)	0.2328(5)	0.2339(5)
$\%_{Sn1}[\%_{Ge1}]$	96[4](4)	92[8](4)	100[0]
$\%_{Ge2}[\%_{Sn2}]$	89[11](4)	84[16](3)	89[11](5)
$\%_{Sn3}[\%_{Ge3}]$	100[0]	100[0]	100[0]
μ_{Fe} (μ_B)	2.06(6)	1.96(4)	2.03(5)
R_{Bragg}, R_f, R_{magn}	2.6, 2.1, 1.7	2.2, 1.9, 5.9	2.0, 2.1, 5.8
χ^2	6.80	9.44	9.34

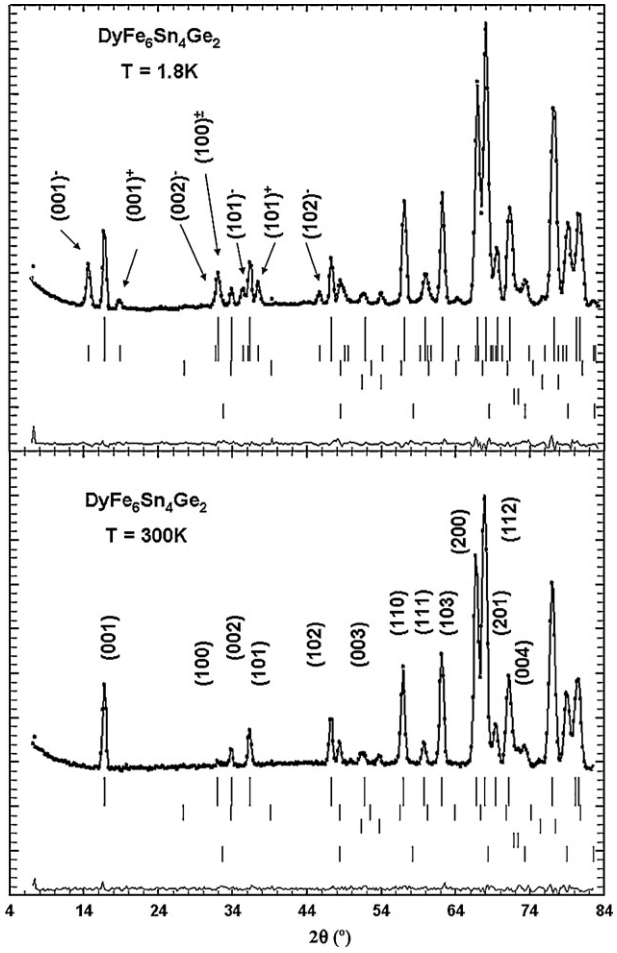

Fig. 2. Observed and calculated neutron diffraction spectra of $DyFe_6Sn_4Ge_2$ at room temperature and at 1.8 K (ticks of extra phases from bottom to top: Fe_3Ge, sample holder, Sn, Dy_2O_3).

3.2. Magnetic structures

The room temperature patterns do not exhibit any extra peaks of magnetic origin thus indicating that all of the magnetic contributions coincide with the nuclear peaks (Figs. 2–4). The refinements of the nuclear structure only show magnetic contributions on the ($h\,k\,l$) peaks with l odd giving evidence of the usual magnetic structures of LFe_6X_6 compounds (X = Ge, Sn) characterized by ferromagnetic Fe Kagomé planes, antiferromagnetically coupled along the stacking direction [1–5,10–17] (Fig. 5). In the present compounds, the absence of a magnetic contribution at the (0 0 l) peaks indicates that the Fe moments are aligned along the hexagonal c axis (Fig. 5). The results of the refinements are gathered in Table 1. At 300 K, the Fe moments are close to 2 μ_B for all three compounds.

At lower temperatures, additional lines appear in the neutron diffraction patterns (Figs. 2–4). In the case of the Dy and Ho compounds, these magnetic lines can be indexed as satellites of the nuclear ones using a propagation vector $Q = (0, 0, q_z)$ as previously reported for $TbFe_6Sn_4Ge_2$ [5]. Preliminary refinements including only the contribution of the lanthanoid sublattice do not account for the very asymmetric intensities of the $(0\,0\,1)^-$ and $(0\,0\,1)^+$ satellites. Therefore, refinements carried out including both a helimagnetic structure for the Ho or Dy moments and, as already observed in $TbFe_6Sn_4Ge_2$, a helimagnetic contribution from of the Fe sublattice. The refined parameters are the lanthanoid moment, the iron helimagnetic component and the phase angle of the Fe sublattice defined as ϕ_{Fe} and $-\phi_{Fe}$ for the Fe moments lying in $z \approx 1/4$ and

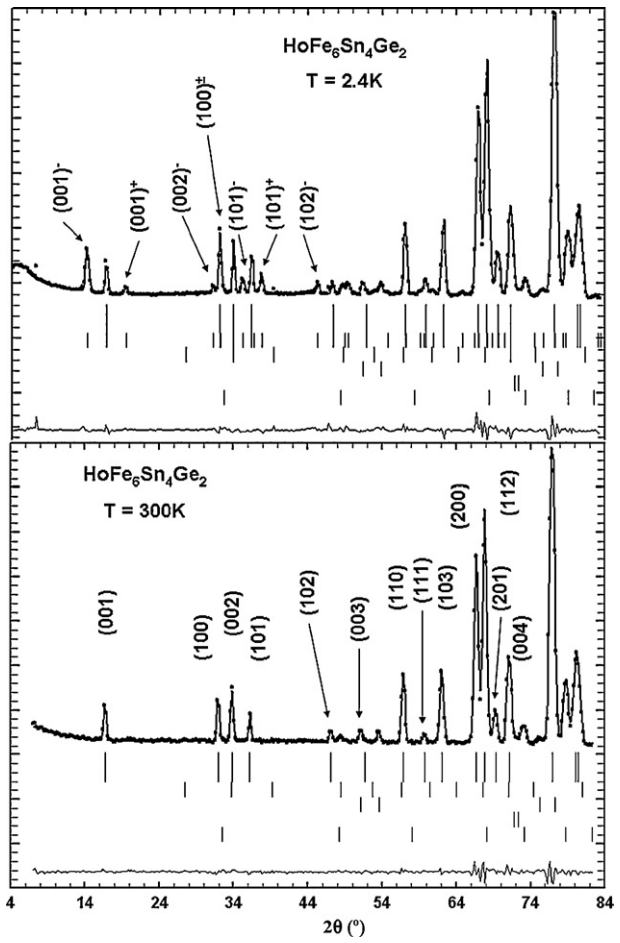

Fig. 3. Observed and calculated neutron diffraction spectra of $HoFe_6Sn_4Ge_2$ at room temperature and at 2.4 K (ticks of extra phases from bottom to top: Fe_3Ge, sample holder, Sn, Ho_2O_3).

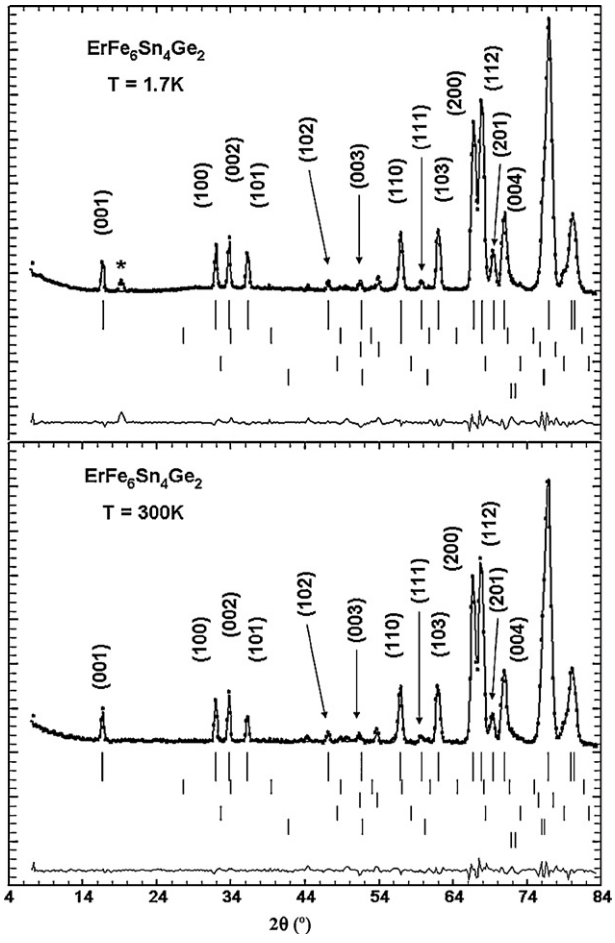

Fig. 4. Observed and calculated neutron diffraction spectra of $ErFe_6Sn_4Ge_2$ at room temperature and at 1.7 K. The asterisk refers to the main magnetic peak of $ErFe_{0.12}Sn_2$ (ticks of extra phases from bottom to top: sample holder, Fe_2Ge, Fe_3Ge, Sn, Er_2O_3).

$z \approx 3/4$ respectively. After these preliminary refinements, attempts to tilt the helical planes of the L and Fe moments were tried, allowing for an angle θ between the normal to helical plane and the c axis (Figs. 6 and 7). In this case, we observed a slight improvement of the reliability factor. The free parameters refined at low temperatures are gathered in Table 2.

The $ErFe_6Sn_4Ge_2$ compound does not exhibit the same additional lines at low temperature. A careful checking of the Bragg angles of the new lines appearing at low temperatures (Fig. 4) showed a fair resemblance with the magnetic lines of the $ErCo_{0.24}Sn_2$ and $ErNi_{0.15}Sn_2$ compounds [18] thus suggesting that they may be due to the magnetic ordering of an $ErFe_xSn_2$ impurity. A neutron diffraction study of a compound $ErFe_{0.12}Sn_2$ confirms this conclusion [19], thus indicating that the Er sublattice in $ErFe_6Sn_4Ge_2$ does not display long range ordering. However, the development of a wide hump around $2\theta = 32^\circ$ suggests the onset of short range ordering.

The thermal variations of the neutron patterns are given in Fig. 8 and show that the ordering of the Dy sublattice takes place in the temperature range 20.3–21.2 K and the ordering of the Ho sublattice in the 11.3–13.4 K range.

The ordering temperatures of the terbium ($T_t = 42$ K [5]), dysprosium and holmium sublattices, display a strong decrease on going to the heaviest lanthanoid compounds, so it is not surprising that erbium is still not ordered at 1.7 K. It is worth noting that the ordering temperatures of the lanthanoid moments determined here are well above those estimated from magnetic measurements in Ref. [9]. We will show in Section 3 that the results of Mössbauer spec-

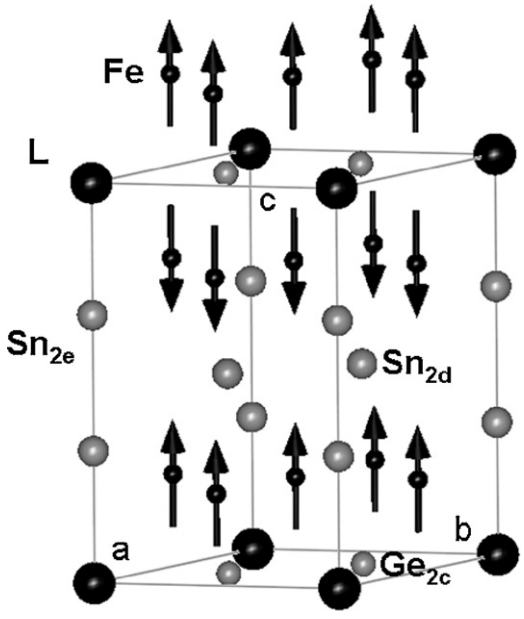

Fig. 5. High temperature antiferromagnetic structure of $LFe_6Sn_4Ge_2$ compounds.

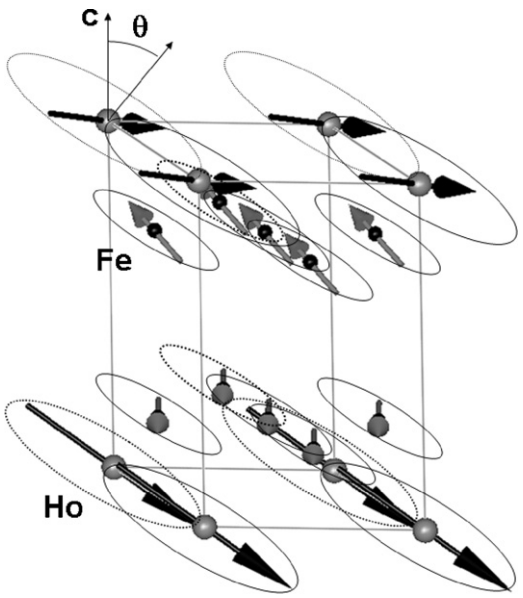

Fig. 6. Representation of the low temperature helimagnetic structure ($HoFe_6Sn_4Ge_2$). The iron helimagnetic component is enhanced for clarity.

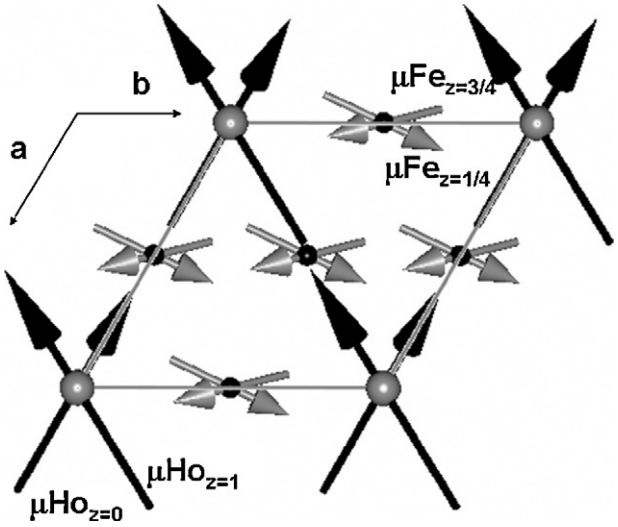

Fig. 7. Low temperature helimagnetic structure ($HoFe_6Sn_4Ge_2$) projected along [0 0 1]. The iron helimagnetic component is enhanced for clarity.

Table 2
Crystallographic and magnetic parameters of $LFe_6Sn_4Ge_2$ refined at low temperature.

L	Dy	Ho	Er
T (K)	1.8	2.4	1.7
a (Å)	5.2649(5)	5.2625(5)	5.2712(5)
c (Å)	8.628(1)	8.627(1)	8.660(1)
z_{Sn}	0.3391(8)	0.339(1)	0.334(1)
z_{Fe}	0.2336(3)	0.2328(5)	0.2344(5)
$\mu_{Fe}(\mu_B)$AF	2.36(3)	2.31(4)	2.33(4)
$\mu_{Fe}(\mu_B)$Heli	0.33(3)	0.27(3)	–
$\mu_L(\mu_B)$Heli	6.32(10)	5.10(12)	–
q_z (r.l.u.)	0.1262(6)	0.1559(7)	–
ϕ (°)	260(10)	263(16)	–
θ (°)	50(1)	36(2)	–
R_{Bragg}, R_f	1.2, 0.9	2.0, 1.3	1.82, 1.56
R_{AF}, R_{heli}	1.9, 5.8	2.9, 11.8	1.77, –
χ^2	30.2	47.5	27.9

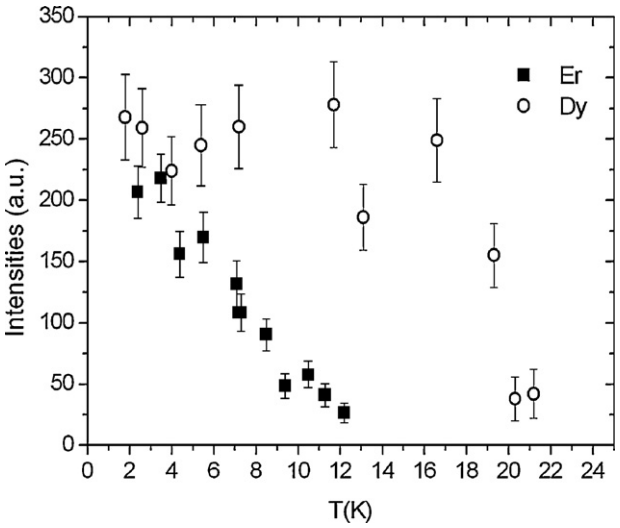

Fig. 8. Thermal variation of the $(0\,0\,1)^-$ satellite for $DyFe_6Sn_4Ge_2$ and $HoFe_6Sn_4Ge_2$.

troscopy are in good agreement with the neutron diffraction results. The magnitude of the Dy and Ho moments is significantly reduced with respect to the theoretical free ion value. The anisotropy direction of the lanthanoid moments is different in terbium compound (easy plane) and in holmium and dysprosium compounds (easy cone).

3.3. Mössbauer spectroscopy

3.3.1. $DyFe_6Sn_4Ge_2$

Visual inspection of the ^{119}Sn Mössbauer spectra of $DyFe_6Sn_4Ge_2$ shown in Fig. 9(a) reveals that the changes associated with the ordering of the Dy moments are quite subtle. The decrease in the magnetic splitting of the Sn(2e) site is small, but as all six lines are well isolated from other features in the spectrum, the drop in B_{hf} is relatively straightforward to fit (Fig. 9(b) (top)). However, the changes in the Sn(2d) component at the centre of the pattern are less clear. There is a significant quadrupole splitting at the Sn(2d) site, and the development of a small hyperfine field presents visually as a loss of definition as the doublet broadens, and as slight reduction in the total intensity. In order to obtain a stable fit to B_{hf}, the quadrupole interaction (Δ) and linewidth for the Sn(2d) site were constrained to the values obtained at 50 K, i.e. above the temperature at which the Dy moments order, and the position of the Sn impurity peak was fixed. When the spectra are fitted using these constraints, a small offset field of 0.22(4) T is observed at 30 and 50 K, where we know that the Dy moments are not ordered. This field provides a measure of the minimum hyperfine field that might reasonably be detected by this method. Further cooling leads to a marked increase in B_{hf}, and it reaches 0.6 T by 5 K (Fig. 9(b) (bottom)). Fitting the temperature dependence of B_{hf}(T) to a $J = 15/2$ Brillouin function (for Dy) yields an ordering temperature of 21(2) K, in agreement with the results of the neutron diffraction analysis above. The hyperfine parameters are gathered in Table 3.

3.3.2. $HoFe_6Sn_4Ge_2$

The lower ordering temperature and smaller moment seen by neutron diffraction in $HoFe_6Sn_4Ge_2$ led us to expect smaller hyperfine field changes in this compound than we observed in $DyFe_6Sn_4Ge_2$. We therefore narrowed the velocity scale by a factor of 2.6 in order to concentrate on the central Sn(2d) feature at the expense of losing most of the peaks from the Sn(2e) sextet. The spectra presented in Fig. 10(a) show that this strategy yields sig-

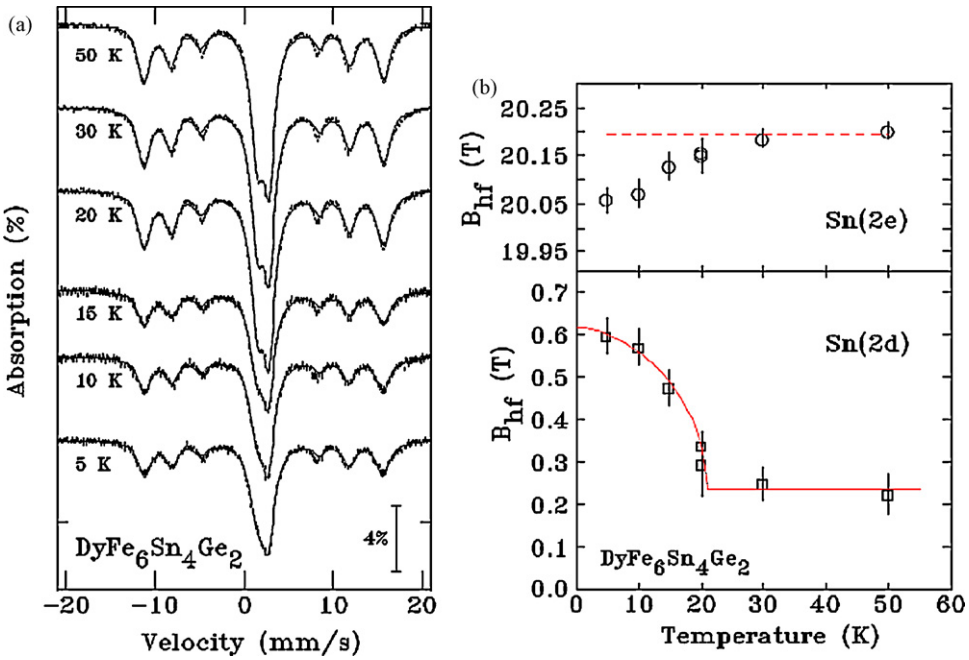

Fig. 9. ^{119}Sn Mössbauer spectra and fitted parameters for $DyFe_6Sn_4Ge_2$. (a) ^{119}Sn Mössbauer spectra of $DyFe_6Sn_4Ge_2$. Solid line is a fit described in the text and (b) temperature dependence of the ^{119}Sn hyperfine field (B_{hf}) at the Sn(2e) site (top), and the Sn(2d) site (bottom) in $DyFe_6Sn_4Ge_2$.

Table 3
Values of the quadrupole splitting (Δ) used for the Sn(2d) component. Also given are the hyperfine fields at 5 K for both the Sn(2c) and Sn(2d) components. No value was obtained for B_{2d}^{hf} for the $ErFe_6Sn_4Ge_2$ compound.

	Temp. (K)	Δ (mm/s) Sn(2d)	Values at 5 K B_{hf} (T)	
			Sn(2c)	Sn(2d)
$DyFe_6Sn_4Ge_2$	50	1.35(1)	20.06(3)	0.60(4)
$HoFe_6Sn_4Ge_2$	20	1.44(1)	19.59(7)	0.32(3)
$ErFe_6Sn_4Ge_2$	35	1.46(1)	19.60(6)	–

nificantly more information about the shape of the central Sn(2d) feature. Remarkably, despite the limited coverage of the Sn(2e) sextet, there was sufficient information available to permit fitting of B_{hf}(T) as long as Δ was held fixed (with only the positions of three of the four central lines of the Sn(2e) sextet observable, it is not possible to determine both the isomer shift and the quadrupole shift for this site). The results of this constrained fit are shown in Fig. 10(b) (top) where the expected slight decline in B_{hf} as the Ho moments order is clearly seen.

Fitting of the central feature from the Sn(2d) site followed the same procedure as used for the $DyFe_6Sn_4Ge_2$ compound above.

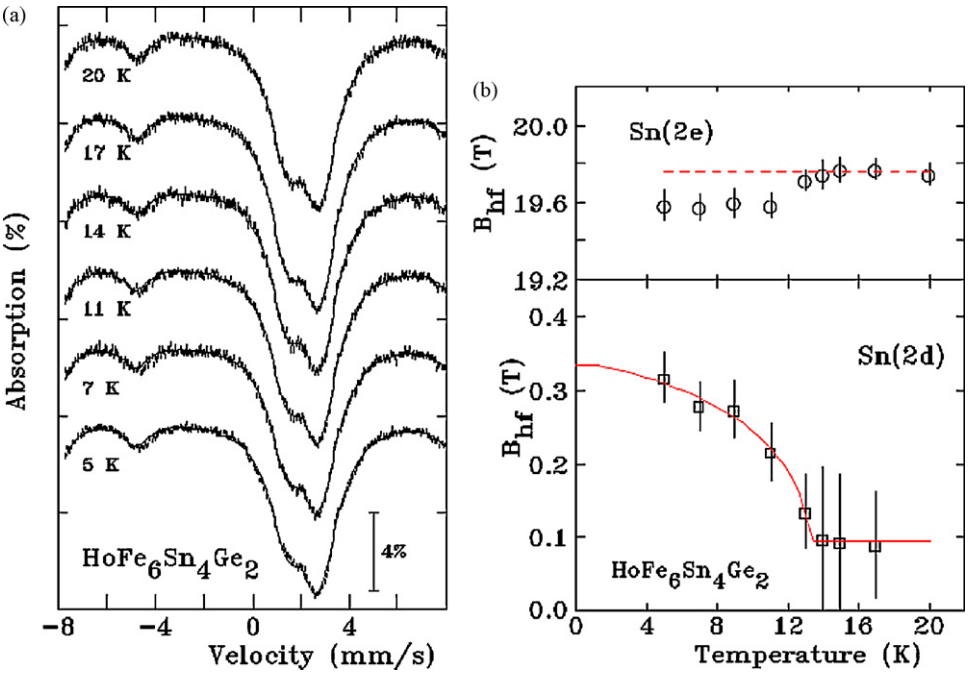

Fig. 10. ^{119}Sn Mössbauer spectra and fitted parameters for $HoFe_6Sn_4Ge_2$. (a) ^{119}Sn Mössbauer spectra of $HoFe_6Sn_4Ge_2$. Solid line is a fit described in the text and (b) temperature dependence of the ^{119}Sn hyperfine field (B_{hf}) at the Sn(2e) site (top), and the Sn(2d) site (bottom) in $HoFe_6Sn_4Ge_2$.

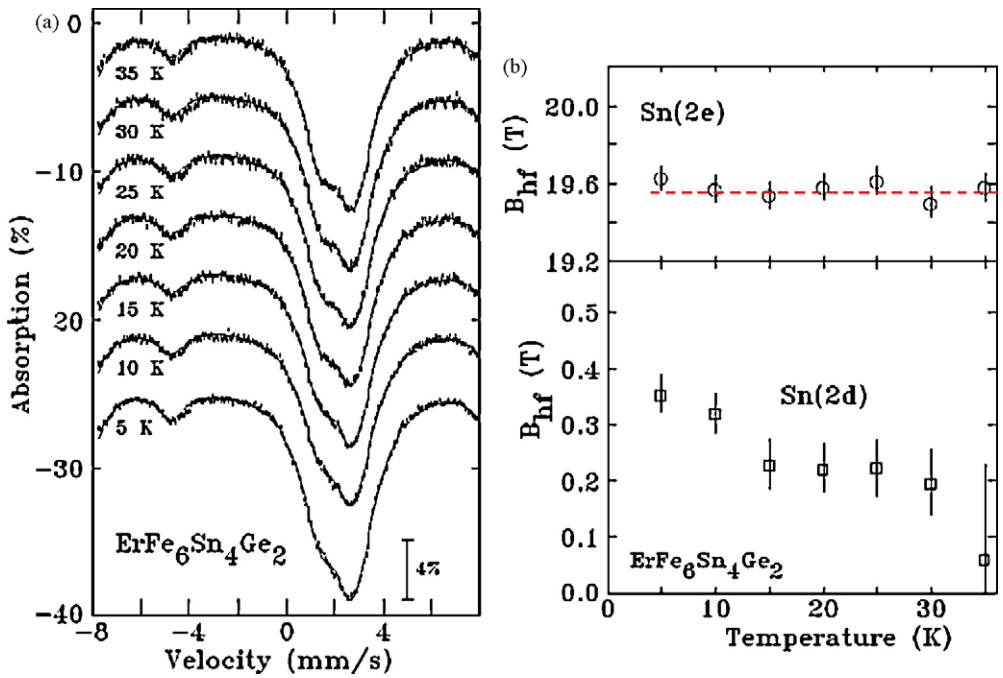

Fig. 11. ^{119}Sn Mössbauer spectra and fitted parameters for $ErFe_6Sn_4Ge_2$. (a) ^{119}Sn Mössbauer spectra of $ErFe_6Sn_4Ge_2$. Solid line is a fit described in the text and (b) TEMPERATURE dependence of the ^{119}Sn hyperfine field (B_{hf}) at the Sn(2e) site (top), and the Sn(2d) site (bottom) in $ErFe_6Sn_4Ge_2$.

The line width and quadrupole splitting were fixed at the values obtained at 20 K, as was the position of the Sn metal impurity. Fitting a hyperfine field with these constraints yielded a non-zero value even where the Ho moments were not expected to be ordered, however at 0.09(7) T, this offset field is much smaller than we saw in $DyFe_6Sn_4Ge_2$ as a result of the improved resolution in the central region. Tracking B_{hf}(T) on further cooling (Fig. 10(b) (bottom)) and fitting it with a $J = 8$ Brillouin function (for Ho) yields an ordering temperature of 13(1) K in full agreement with the results of the neutron diffraction analysis above.

3.3.3. *$ErFe_6Sn_4Ge_2$*

The ^{119}Sn Mössbauer spectra of $ErFe_6Sn_4Ge_2$ shown in Fig. 11(a) show essentially no changes beyond what can be attributed to the expected growth of the metallic tin impurity component on cooling. Analysis of the spectra following the same procedures as used for the Dy and Ho compounds yields the results plotted in Fig. 11(b). No change in the hyperfine field is observed for the Sn(2e) component between 5 and 35 K. While some changes in the fitted field for the Sn(2d) are apparent in Fig. 11(b) (bottom), the offset field is quite large (0.22(4) T) and the observed line width for this component was ≈0.15 mm/s larger than in the other two compounds. Fits done without a hyperfine field yielded better χ^2 values at all temperatures. Taken with the results of the neutron diffraction data and the absence of a change at the Sn(2e) site, these results lead us to conclude that the Er moments in $ErFe_6Sn_4Ge_2$ do not order above 5 K.

4. Discussion

The hexagonal $LFe_6Sn_4Ge_2$ compounds display the same AF magnetic order of the iron sublattice characterized by ferromagnetic (0 0 1) planes antiferromagnetically coupled along the [0 0 1] direction with the sequence +−+−. In all cases, the Fe moment is close to 2.35 μ_B at 2 K and an easy axis magnetisation direction prevails. This kind of magnetic ordering is usually observed in other orthorhombic LFe_6X_6 compounds and this resemblance results from the similar arrangement of the iron atoms in all these structures [20]. In addition, it is worth noting that the significant changes in the Fe–Fe interlayer distances due to the replacement of Sn by Ge does not appear to affect this arrangement.

More interestingly, the stabilisation of the same hexagonal $HfFe_6Ge_6$ structure for all the $LFe_6Sn_4Ge_2$ compounds simplifies the comparison of the magnetic behaviour of the L sublattice in each compound since the crystallographic arrangement of the L atoms is now the same in all compounds studied. This simplification does not occur in the orthorhombic phases previously studied as they are characterized by different tridimensional arrangements of the lanthanoid atoms [20].

We found that all magnetically ordered compounds display similar magnetic structures characterized by ferromagnetic lanthanoid (0 0 1) planes and a helimagnetic arrangement along [0 0 1] with a turn angle (α_L) ranging between 34.7(1)° for the terbium compound to 56.2(2)° for the holmium compound (see Fig. 7). This angle is rather weak suggesting that the lanthanoid magnetic sublattice is close to ferromagnetism, a view which is consistent with the weak critical fields observed by magnetisation measurements [9]. In addition, all magnetic structures are characterized by a helimagnetic component of the iron sublattice decreasing from 0.40(4) μ_B in the terbium compound to 0.33(3) and 0.27(3) μ_B in the dysprosium and holmium compounds.

The appearance of this helimagnetic component is linked to the L ordering and therefore reflects an exchange interaction between the Fe and lanthanoid moments which in turn should be proportional to the quantity $(g-1)\langle J\rangle M_{Fe}$, decreasing rapidly on going from Tb to Er. This effect might explain the corresponding decrease in the magnitude of the helimagnetic component i.e. the ability to deform the AF iron sublattice also decreases in the same manner.

The angles between the lanthanoid moments and the helimagnetic iron component belonging to the successive (0 0 1) planes are more intriguing. These angles are related to the q_z component of the propagation vector and to the refined phase angle ϕ_{Fe}. They are gathered in Table 4 and Fig. 12 displays the evolution of the corresponding cosine values as a function of the lanthanoid element. It is worth noting that only the angle between the L moment and the Fe moment belonging to the next nearest Fe plane is consistent across

Table 4
Characteristic angles of the helimagnetic structure of the $LFe_6Sn_4Ge_2$ compounds (the angles of the successive L moments are given by $\alpha_{L0+n} = 360z_L q_z$ and the angles of the successive Fe moments are given by $\alpha_{Fe1/4+n} = 360z_{Fe}q_z + \phi_{Fe}$ and $\alpha_{Fe3/4+n} = 360z_{Fe}q_z - \phi_{Fe}$; β is the angle between the moments belonging to different planes; $\sum \vec{\mu}_{Fe}$ and $\sum \vec{\mu}_L$ are the vector sum of the Fe and R moments surrounding the Sn(2d) site).

L	q_z	ϕ_{Fe} (°)	$\alpha_{Fe1/4}$ (°)	$\alpha_{Fe3/4}$ (°)	$\alpha_{Fe5/4}$ (°)	$\alpha_{L4/4}$ (°)	$\beta_{L0-Fe1/4}$ (°)	$\beta_{L0-Fe3/4}$ (°)	$\beta_{L0-Fe5/4}$ (°)	$\beta_{Fe1/4-Fe3/4}$ (°)	$\mu_{Fe\ heli}$ (μ_B)	$\sum \vec{\mu}_{Fe}$	$\beta_{L0L4/4}$ (°)	μ_{L_heli} (μ_B)	$\sum \vec{\mu}_L$
Tb	0.0963	230	238.2	−203.5	272.8	34.7	238.2	−203.5	272.8	81.7	0.40	0.605	34.7	6.84	13.05
Dy	0.1262	260	270.6	−225.2	316.0	45.4	270.6	−225.2	316.0	135.8	0.33	0.248	45.4	6.32	11.66
Ho	0.1559	263	276.1	−219.9	332.2	56.1	276.1	−219.9	332.2	136.0	0.27	0.202	56.1	5.10	9.00

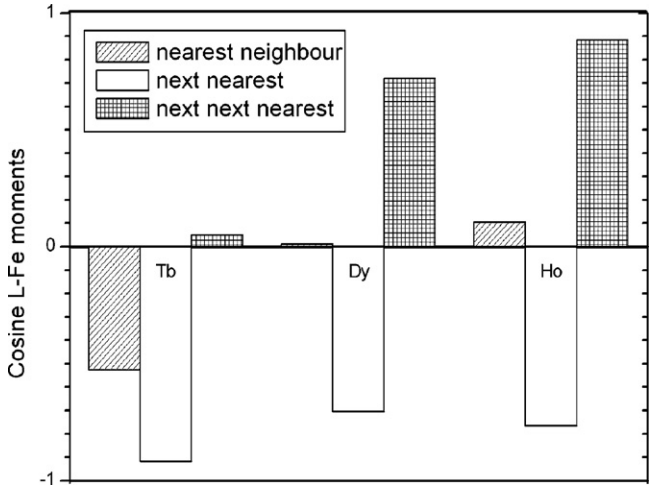

Fig. 12. Cosine of the angle between the L moment and the nearest neighbour, next nearest neighbour and next next nearest neighbour iron planes for the three compounds $LFe_6Sn_4Ge_2$ (L = Tb, Dy, Ho).

the whole L series. This is in contrast with the known helimagnetic LMn_6X_6 compounds for which the angle between the L moment and the Mn moment belonging to the *nearest* Mn plane is always close to 180° [21,22]. This suggests that, in the iron compounds, the next nearest neighbour interaction is greater than the nearest neighbour interaction. As the corresponding interlayer distance is relatively large, we would expect the next nearest neighbour to be quite weak. The apparent independent ordering of the L moments in the orthorhombic LFe_6X_6 compounds reported in previous papers and also the small magnitude of the helimagnetic component in the hexagonal $LFe_6Sn_4Ge_2$ compounds might be related to this effect. Therefore, the behaviour of the iron compounds is only related to the strongly antiferromagnetic character of the Fe sublattice but also to particularly weak L–Fe interactions.

The Mössbauer results agree with the results of neutron diffraction and confirm the conclusions of this technique. In the high temperature range, only the Sn(2e) site experiences a transferred field since the Sn(2e) site is close to one ferromagnetic iron plane (Figs. 1 and 2). On the contrary, the Sn(2d) site is halfway between two antiferromagnetically coupled iron planes and so it does not experience transferred hyperfine field. At low temperatures, the Sn(2e) site is affected by the slight reorientation of the iron moment and the development of an ordered magnetic moment on the nearby L site. This leads to the small decrease of the hyperfine field and the change of the quadrupolar shift observed in $TbFe_6Sn_4Ge_2$ [5]. Similarly, the helimagnetic ordering of the Fe sublattice means that the two Fe layers surrounding the Sn(2d) sites are no longer perfectly antiparallel and a small net transferred hyperfine field develops. There is also a contribution from the ordered L moments in the next nearest neighbour planes.

Table 4 gives the vector sum of the surrounding helimagnetic Fe and L components. For both quantities, we observe a decrease on going from Tb to Ho that corresponds with the decrease of the transferred hyperfine field seen at the Sn(2d) nucleus. However, the weakness of the hyperfine fields does not allow an estimation of the relative contribution of the two sublattices to the total transferred field.

5. Conclusions

The neutron diffraction study of the compounds $DyFe_6Sn_4Ge_2$ and $HoFe_6Sn_4Ge_2$ has shown that they behave like the previously studied compound $TbFe_6Sn_4Ge_2$. Comparison of the refined magnetic parameters in the three compounds suggests that the

exchange between the lanthanoid and iron moments is dominated by the interaction between the next nearest neighbours. It would be interesting to check this hypothesis by a study of other suitable compounds or solid solutions. As the transferred hyperfine field at the 2(c) site is expected to be dominated by the effects of the L sublattice, a Mossbauer study of intermediate solid solutions in which the 2(c) e is partially occupied by tin atoms may yield some useful insights.

Acknowledgements

We are grateful to the Institut Laue Langevin (Grenoble) for the provision of research facilities facilities and to Dr Bachir Ouladdiaf for his help during the recording. DHR and LKP were supported by grants from the Natural Sciences and Engineering Research Council of Canada and Fonds Québécois de la Recherche sur la Nature et les Technologies. C.J. Voyer and E. Alonso-Ortiz (McGill) assisted with the collection of the ^{119}Sn spectra.

References

[1] J.M. Cadogan, D.H. Ryan, J. Alloys Compd. 326 (2001) 166.
[2] J.M. Cadogan, D.H. Suharyana, D.H. Ryan, O. Moze, W. Kockelmann, IEEE Trans. Magn. 37 (4) (2001) 2006.
[3] D.H. Ryan, J.M. Cadogan, J. Appl. Phys. 79 (8) (1996) 6004, 2B.
[4] J.M. Cadogan, D.H. Ryan, O. Moze, D.H. Suharyana, M. Hofmann, J. Phys. Condens. Matter 15 (10) (2003) 1757–1771.
[5] L.K. Perry, D.H. Ryan, G. Venturini, B. Malaman, J. Alloys Compd. 436 (1–2) (2007) 1–8.
[6] M. François, G. Venturini, B. Malaman et, B. Roques, J. Less Common Met. 160 (1990) 197–213.
[7] J. Rodriguez-Carvajal, Physica B 192 (1993) 55.
[8] C.J. Voyer, D.H. Ryan, Hyperfine Interact. 170 (2006) 91.
[9] G. Venturini, J. Alloys Compd. 400 (2005) 37.
[10] T. Mazet, B. Malaman, J. Magn. Magn. Mater. 219 (2000) 33.
[11] P. Schobinger-Papamantellos, K.H.J. Buschow, F.R. de Boer, C. Ritter, O. Isnard, F. Fauth, J. Alloys Compd. 267 (1–2) (1998) 59.
[12] O. Oleksyn, P. Schobinger-Papamantellos, J. Rodriguez-Carvajal, E. Brück, K.H.J. Buschow, J. Alloys Compd. 257 (1997) 36.
[13] J.M. Cadogan, D.H. Ryan, I.P. Swainson, J. Phys. Condens. Matter 12 (2000) 8963.
[14] J.M. Cadogan, D.H. Ryan, I.P. Swainson, O. Moze, J. Phys. Condens. Matter 10 (24) (1998) 5383.
[15] O. Zaharko, P. Schobinger-Papamantellos, J. Rodriguez-Carvajal, K.H.J. Buschow, J. Alloys Compd. 288 (1–2) (1999) 50.
[16] O. Zaharko, P. Schobinger-Papamantellos, C. Ritter, J. Rodriguez-Carvajal, K.H.J. Buschow, J. Magn. Magn. Mater. 187 (1998) 293.
[17] T. Mazet, B. Malaman, J. Phys. Condens. Matter 12 (6) (2000) 1085.
[18] B. Penc, E. Wawrzynska, A. Szytula, A. Gil, J. Hernandez-Velasco, A. Zygmunt, J. Alloys Compd. 375 (2004) L1.
[19] G. Venturini, unpublished, 2009.
[20] B. Chafik El Idrissi, G. Venturini, B. Malaman, Mater. Res. Bull. 26 (12) (1991) 1331.
[21] P. Schobinger-Papamantellos, G. André, J. Rodriguez-Carvajal, J.H.V.J. Brabers, K.H.J. Buschow, J. Alloys Compd. 226 (1995) 113.
[22] C. Lefèvre, G. Venturini, B. Malaman, J. Alloys Compd. 346 (2002) 84.